Journal of Neuropathology and Experimental Neurology
Vol. 62, No. 11
November, 2003
pp. 1154–1165

Periventricular/Intraventricular Hemorrhage in Neonatal Mouse Cerebrum

MENGZHOU XUE, MD, JANANI BALASUBRAMANIAM, MSC, RICHARD J. BUIST, PHD, JAMES PEELING, PHD, AND MARC R. DEL BIGIO, MD, PHD, FRCPC

Abstract. Periventricular/intraventricular hemorrhage (PVH/IVH) into brain can occur in premature infants and is associated with poor developmental outcome. The purpose of this study was to develop and characterize a model of PVH/IVH in newborn mouse. We hypothesized that periventricular germinal matrix would exhibit reduced cell proliferation. PVH/IVH was induced in 1-day-old mice by injection of autologous blood into the periventricular tissue. Magnetic resonance images (MRI) were obtained from 15 minutes to 14 days later. Mice were killed 4 hours to 28 days later. Cell proliferation, dying cells, astrocyte and microglial reactions, neutrophils, and lymphocytes were quantified. Histological studies showed that MRI accurately localizes the hematoma but overestimates its size. The hematoma, located in the striatum and germinal tissue, always extended into the lateral ventricles. Cell proliferation, measured by Ki67 immunoreactivity, was suppressed bilaterally in germinal matrix and beyond from 8 hours to 7 days. Increased cell death was observed in the ipsilateral striatum and germinal matrix 1 and 2 days after PVH/IVH. Astrocyte and microglia reaction peaked at 2 days and persisted up to 28 days. Inflammatory response was minimal. Extravasated blood might play an important role in brain damage following PVH/IVH through suppression of cell proliferation.

Key Words: Cell death; Cell proliferation; Immunohistochemistry; Inflammation; Ki67; Magnetic resonance imaging (MRI); Periventricular/intraventricular hemorrhage (PVH/IVH).

INTRODUCTION

Periventricular/intraventricular hemorrhage (PVH/IVH) is defined as hemorrhage originating primarily from subependymal germinal matrix (GM) with extension into the ventricles. It occurs most commonly in premature infants 24 to 30 weeks gestation (1). The pathogenesis of PVH/IVH is multifactorial and consists of a combination of varying arterial and venous blood flow (1–3), coagulation disturbances (4, 5), veins with fragile walls in the germinal matrix (1), and excessive fibrinolytic activity in the immature brain tissue (3). Perinatal brain damage is among the most prevalent and costly forms of neurologic disability (6, 7). PVH/IVH can be associated with hemiplegic cerebral palsy (8), mental retardation (9), and hydrocephalus (1, 7). Hemorrhage causes brain damage through direct tissue destruction, followed by secondary damage to cells through proteolytic activity of enzymes involved in blood clot formation, as well as lysis, inflammation and cytokine production, edema, and hemoglobin released from lysed erythrocytes (10–12). Some of these mechanisms have been studied experimentally in adult brains. However, unlike damage due to hypoxia-ischemia which has been studied extensively (13), neonatal brain hemorrhage has been largely ignored (2).

The periventricular GM consists of pluripotential cells that give rise largely to cerebral neurons before 20 weeks gestation in humans and later to precursors of oligodendrocytes and astrocytes (1). In humans the GM involutes by about 34 to 38 weeks gestation. In the mouse and rat, periventricular germinal cells generate neurons prior to birth and glial cell precursors during the week after birth (14–16). Experimental studies have shown that plasticity is not very effective in the newborn rodent brain, likely because normal developmental processes are interrupted (17). Hypoxic ischemic damage to 7-day rat brain, in which the GM has largely involuted, reduces the quantity of oligodendrocyte precursors (18). In humans we have observed that hemorrhage is associated with suppression of germinal cells in cell cycle (Fig. 1). Because reduced brain cell production could have important consequences, our goal was to develop and characterize a novel animal model of PVH/IVH in which we could test the hypotheses that GM cell proliferation is reduced after PVH/IVH. We used 1- to 2-day-old mice based upon the state of the subependymal zone/ganglionic eminence, which is roughly comparable to that in 24 to 26 week gestational age human brains (19, 20). Magnetic resonance imaging (MRI) was used to standardize the hematoma for successive time point analyses of the mouse brain following PVH/IVH.

MATERIALS AND METHODS

Animal Model

All experimental procedures were done in accordance with guidelines of the Canadian Council on Animal Care. Protocols were approved by the local experimental ethics committee. A

From the Departments of Pathology (MX, JB, MRD) and Radiology (RJB, JP), University of Manitoba, and Manitoba Institute of Child Health (MX, JB, MRD), Winnipeg, Canada.

Correspondence to: Marc R. Del Bigio, MD, PhD, FRCPC Department of Pathology, University of Manitoba 770 Bannatyne Ave, Winnipeg, MB, R3E 0W3, Canada. E-mail: delbigi@cc.umanitoba.ca

This work was supported by grants to Dr. Del Bigio from the Heart and Stroke Foundation of Manitoba, Manitoba Health Research Council, and Children's Hospital Foundation. Dr. Del Bigio holds the MMSF Clinical Research Professorship. Mengzhou Xue and Janani Balasubramaniam have Doctoral Research Awards from CIHR/HSFC.

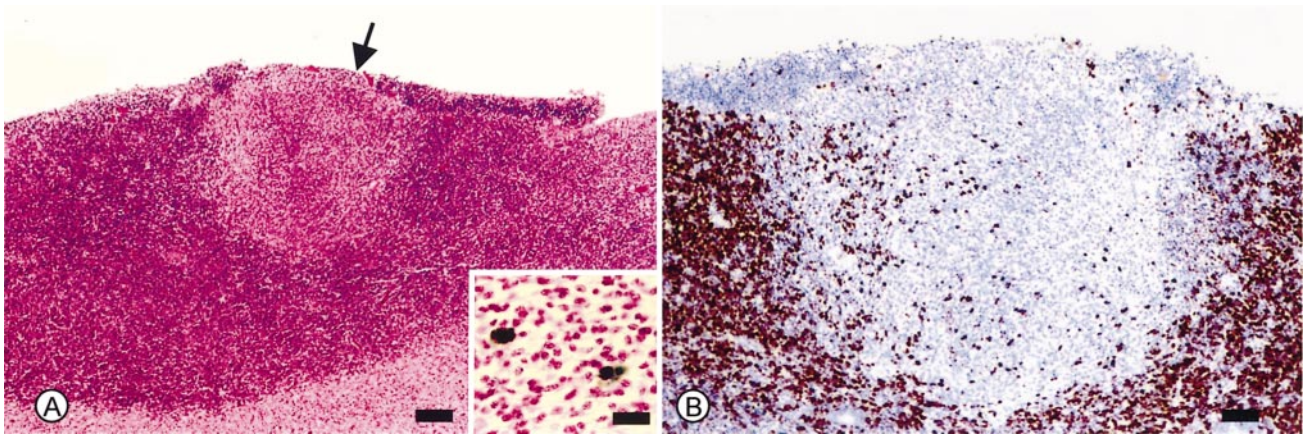

Fig. 1. **A:** Photomicrograph showing periventricular germinal tissue (ganglionic eminence) of a human fetus (~24 weeks gestational age) a few days after a small periventricular hemorrhage. There is a circular area of decreased cellularity along the ventricle wall (arrow) (H&E stain) (Bar = 100 μm). This was shown to be the site of hemorrhage by the presence of hemosiderin-containing macrophages (inset, Perl's stain for iron) (Bar = 25 μm). **B:** Immunohistochemical labeling of an adjacent section with anti-Ki67 antibody demonstrates that the damaged area has a greatly reduced proportion of proliferating cells (brown nuclei) (Bar = 50 μm).

total of 118 locally bred newborn (24–36 hours) CD-1 mice weighing 1.42 to 1.95 grams were used. The mice were anesthetized with 1.5% to 2% halothane in a 70:30 mixture of N_2O:O_2. Autologous whole blood (15 μL) was collected in a sterile syringe by placing the tail in warm water for 1 min, cleaning the skin with 70% alcohol, and cutting the tail tip. Because the mice could not be secured in a stereotaxic frame, the injections of blood were done freehand with the needle inserted percutaneously. A 27-gauge needle was attached to the syringe and quickly introduced into the right periventricular region of the newborn mouse (1 mm lateral, 0.5 mm behind the right eye, 3 mm deep to the scalp surface). A shield around the needle stabilized it against the scalp and ensured correct depth of penetration. Blood (15 μL) was injected over 1 min; the needle was left in the place for 10 to 20 seconds, and then removed slowly. Mice were returned to the mother after the 3-min procedure. Sham controls consisted of 12 newborn CD-1 mice into which 15 μL sterile saline was injected. Because needle insertion alone also can cause hemorrhage, 25 intact mice were also used as controls following halothane anesthesia only. Physiological monitoring was not possible. To compare the extent of blood spread, 5 additional adult CD-1 mice (weight 20–25 grams) underwent autologous whole blood (50 μL) injection. The method was similar except the head was affixed in a stereotaxic frame.

Magnetic Resonance Imaging

Proton MRI was carried out using a Bruker Biospec/3 MR scanner equipped with a 21-cm bore magnet operating at a field of 7 Tesla (Bruker BioSpin GmbH, Karlsruhe, Germany). The MR probe used was a custom-built quadrature volume coil (length 3.0 cm, inside diameter 2.0 cm) (21). The mouse pups were anesthetized with 1.5% to 2% halothane in a 70:30 mixture of N_2O:O_2 and maintained normothermic by blowing warm air over the animal holder. Scout MR scans were taken with a magnetization transfer prepared TurboFLASH (MT-FLASH) sequence with a TR of 3.7 ms, TE of 2.3 ms, field of view of 4.0 × 4.0 cm^2, slice thickness of 1.0 mm, and matrix size of 128 × 128 pixels. Applying a 2-second continuous-wave RF pulse at an offset of 12,000 Hz and strength of 25 mT effected the magnetization transfer. High-resolution scans were taken with a standard multi-slice spin-echo sequence using TRs in the range of 800 to 2,500 ms, TEs of either 7.2, 60, or 120 ms, field of view of 3.0 × 3.0 cm^2, slice thickness of 1.0 mm, and matrix size of 256 × 256. Our predominant interest was to observe the signal loss due to the injected blood. This was dramatic even at very short TE (7.2 ms). We found that the T1-weighting produced by the short TR was far less than the T2-contrast produced by the paramagnetic relaxation effect. Therefore, the short TR was chosen for most scans to reduce the overall scan time. Mice were only used for subsequent histological analysis if MRI showed a standard hematoma size and location.

The volume of the acute hematoma observed by MRI and histology was compared. For this we used 13 mice, 4 of which were imaged twice at 15 to 30 min and 4 hours. Four had MRI and histology compared at 15 to 30 min, and 9 were compared at 4 hours. On MR images the area of signal alteration was traced and measured by computerized planimetry. The total volume proportion was calculated based on 1-mm slice thickness. Histologic sections every 200 μm encompassed the entire hematoma site. Camera lucida tracing was used to measure the blood collections on each slice, including intraventricular blood and parenchymal hematoma. The total volume of extravasated blood was then calculated.

Histologic Evaluation

Mice were reanesthetized at 4 and 8 hours, 1, 2, 7, and 28 days (4–5 mice were used for each time point) after blood injection into brain, or 8 hours, 1, 2, 7 days (3–4 mice were used for each time point) after saline injection. They were perfused through the heart with 5 to 20 ml ice-cold 4% paraformaldehyde in 0.1 mol/L phosphate buffered saline (PBS). The brain was removed and stored in the same fixative for 1 to 10 days.

TABLE
Summary of Immunohistochemical and Histochemical Staining Used

Antibody/histochemical method	Specificity	Dilution	Source
Hamster anti-mouse CD3ε monoclonal (biotin-conjugated)	T lymphocytes	1/300	Pharmingen Canada, Inc., Mississauga, ON
Rat anti-mouse CD3	T lymphocytes	1/100	Pharmingen
Rat anti-mouse CD4	Helper T cells	1/300	Pharmingen
Rat anti-mouse CD8 (Ly-2)	Cytotoxic T cells	1/100	Pharmingen
Rat anti-mouse Ly-6G (Gr-1)	Neutrophils	1/500	Pharmingen
Rabbit anti-cow GFAP	Astrocytes	1/1000	Dako Corp., Carpinteria, CA
Rabbit anti-Ki67	Proliferating cells	1/500	Novocastra Laboratories, Newcastle, UK
Ricinus communis agglutinin lectin (RCA-1) (biotin-conjugated)	Microglia	1/2000	Sigma, St. Louis, MO
TUNEL	Dying cells	—	Intergen, Purchase, NY
Fluoro-Jade B	Dying neurons	—	Histo-Chem, Inc., Jefferson, AR

Fixed brains were cut coronally to surround the injection sites, and slices were dehydrated and embedded in paraffin. Sections (6 μm) were cut serially for the whole brain and each tenth section was stained with hematoxylin and eosin (H&E). Near the lesion center, where the brain damage was maximal, a variety of histological and immunohistochemical stains were performed (see below).

We wanted to investigate the inflammation that occurs after PVH/IVH, but the relevant antigens cannot be detected reliably on paraffin sections. Therefore, additional mice were reanesthetized at 2, 4, 7, 14, and 28 days (4–5 mice were used for each time point) after blood injection into brain, perfused through the heart with 5 to 20 ml ice-cold 0.15 mol/L PBS, following by 5 to 20 ml ice cold 10% sucrose in 0.1 mol/L phosphate buffer. The brain and spleen were removed and stored in 10% sucrose in 0.1 mol/L PB with 0.02% sodium azide for 3 to 8 days. Brains were cut coronally approximately 3 to 4 mm on either side of the lesion center. Frozen sections (14 μm) were cut serially through the anterior half of the cerebrum. Selected levels were stained with H&E. Near the lesion center, a variety of immunolabeling procedures were performed using anti-CD3, anti-CD3ε, anti-CD4, anti-CD8, and anti-Gr-1 antibodies to detect the lymphocyte and neutrophil infiltration (Table). Anti-CD3ε antibody was used to detect lymphocytes in the frozen brain tissues by labeling the T cell receptor associated CD3 complex, which is expressed on thymocytes and mature T lymphocytes of all mouse strains (22). Frozen sections were fixed in −20°C acetone, washed, blocked with 10% donkey serum, and incubated with biotin-conjugated hamster anti mouse CD3ε monoclonal antibody (diluted 1/300 in 1% bovine serum albumin) at 4°C overnight. Slides were then washed, incubated in streptavidin-peroxidase HRP (1/400) (Dako Corp., Carpinteria CA), washed, colored with diaminobenzidine (Sigma, St. Louis, MO)-H_2O_2 solution, washed and coverslipped. Purified rat anti-mouse CD3, anti-mouse CD4, anti-mouse CD8, and anti-mouse Gr-1 antibodies were used to detect infiltration of lymphocytes and neutrophils on frozen brain sections by immunofluorescence. Frozen sections were fixed in −20°C acetone, washed, blocked with 10% donkey serum, and incubated with rat anti mouse monoclonal antibodies at 4°C overnight. Slides were then washed and incubated in mouse anti rat Cy3 (Jackson ImmunoResearch Laboratories Inc., West Grove PA), coverslipped with mounting media for fluorescence microscopy (Kirkegaard & Perry Laboratories, Gaithersburg MD), and observed by fluorescence microscopy. For all antibodies procedures negative control sections were processed with omission of the primary antibody. Positive controls were pieces of spleen tissue embedded adjacent to the brain.

Ricinus communis agglutinin lectin (RCA-1) labeling was used to demonstrate reactive microglial cells (23). Paraffin sections were dewaxed and rehydrated, washed, quenched with 0.3% H_2O_2, blocked with 10% normal sheep serum, and incubated with biotinylated lectin (diluted 1/2,000) (Vector Laboratories, Inc., Burlingame CA). Slides were then washed, incubated with streptavidin-peroxidase (1/400), colored with diaminobenzidine—H_2O_2 solution, washed, and coverslipped. Control sections were processed with omission of the biotinylated lectin.

Anti-glial fibrillary acidic protein (GFAP) antibody was used to evaluate astrocyte reaction. Paraffin sections were dewaxed, rehydrated, quenched with 0.3% H_2O_2, blocked with 10% normal goat serum, and incubated with rabbit anti-GFAP polyclonal antibody at 4°C overnight. Slides were then washed, incubated with biotinylated goat anti-rabbit IgG (1/300) (Jackson ImmunoResearch), streptavidin-peroxidase (1/400), and colored with diaminobenzidine—H_2O_2 solution. Control sections were processed with omission of the primary antibody.

Detection of Proliferating Cells and Dying Cells

Cell proliferation status in the brain was assessed with an antibody that recognizes nuclear Ki67 antigen, which is expressed from late G1 to M phase of the cell cycle (24). Bisbenzimide (2-(4-ethoxyphenyl)-5-(4-methyl-1-piperazinyl)-2,5-bi-1H-benzimidazole trihydrochloride; Hoechst 33342, Sigma) counterstaining was used to show all nuclei. Paraffin sections were dewaxed and rehydrated. Slides were microwaved in 0.6 M citric acid buffer for 15 min and were cooled in 0.1 M PBS for 20 min. Slides were blocked with 10% normal donkey serum and incubated with rabbit anti-Ki67 polyclonal antibody at 4°C overnight. Slides were then washed, incubated with Cy3 donkey anti-rabbit IgG (1/500) (Jackson ImmunoResearch), and

coverslipped. Negative controls were processed without the primary antibody.

TUNEL (terminal deoxynucleotidyl transferase (TdT)-mediated deoxyuridine triphosphate (dUTP)-biotin nick end labeling) was used to identify dying cells with damaged DNA. Paraffin embedded sections were dewaxed and rehydrated, then incubated in 20 μL/ml proteinase K for 15 min. TUNEL was accomplished using Apoptag in situ kit (Intergen, Purchase, NY). After immersion in equilibration buffer for 10 min, sections were incubated with TdT and dUTP-digoxigenin in a humidified chamber and then incubated in the stop/wash buffer. Sections were washed before incubation in anti-digoxigenin-peroxidase solution (1/500 in PBS), and colored with diaminobenzidine—H_2O_2 solution. Sections were counterstained with methyl green. Negative control sections were treated similarly but incubated in the absence of TdT enzyme or dUTP-digoxigenin.

Sections of brain were stained with Fluoro-Jade to show dying neurons (25, 26) by incubating sections in 0.06% potassium permanganate for 15 min while gently shaking on a rotating platform. Then 0.001% Fluoro-Jade (Histo-Chem, Inc., Jefferson, AR) staining solution was applied for 30 min, following by PBS washing, air drying, and coverslip application.

Determination of Hematoma Size and Cell Counts

The coronal levels with damage were identified. A ''camera lucida'' drawing was used to trace the damaged areas, defined by the presence of blood, tissue rarefaction, or necrosis. Computerized planimetry was used to measure the traced areas. Using an ocular reticule and ×400 ocular magnification, TUNEL-positive dying cells, extravascular neutrophils identified on H&E sections by characteristic nuclear morphology, and RCA-1-labeled cells were counted in 4 fields (each area 540 μm × 540 μm) immediately adjacent to the damage site including striatum and GM as previous described (27). Areas with large blood vessels were avoided. The GFAP-positive cells were assessed semiquantitatively by using 4 grades (0, no positive cells; 1, rare positive cells; 2, moderate number positive cells; and 3, many positive cells). The proportion of cells in cycle was calculated by dividing the number of Ki67 immunoreactive nuclei by the total number of nuclei stained with bisbenzimide. These proportions were determined in germinal matrix (3 areas comprised of four 540 μm × 540 μm fields each, objective ×40 magnification). Cells were also counted in striatum, white matter, and cerebral cortex (superficial and deep cortex) in 2 fields each (each 1.08 μm × 1.08 μm, objective ×20 magnification). All counts were made by an observer blinded to the time after injection. For acute experiments, the presence of blood precluded blinding between groups.

Statistics

All data are expressed as mean ± SEM. Data were analyzed to ensure normal distribution. Intergroup comparisons were made by ANOVA followed by Fisher least square difference test. A difference of $p < 0.05$ was considered significant. Nonparametric data (i.e. GFAP) were assessed using Kruskall-Wallis test. We used StatView 5.01 software (SAS Institute, Cary, NC).

RESULTS

MRI of PVH/IVH in Newborn Mice

All mice tolerated the 15-μL injection of blood into the periventricular tissue well and there was no surgical mortality. On T2-weighted MR images, blood appeared dark (Fig. 2A–D) due to the large susceptibility effect of paramagnetic hemoglobin products. The blood appeared to spread widely and rapidly following injection into the periventricular region. In the majority of mice, blood entered the lateral ventricles. Bright regions surrounding the ventricles on T2-weighted images are likely due to susceptibility artifact. This was confirmed by switching the read and phase encoding gradients in imaging studies carried out 1 day after PVH/IVH (data not shown). When the read gradient was directed left-right (L-R) and phase-encoding anterior-posterior (A-P), the bright artifact appeared to the right and left of the hematoma; when the read gradient was A-P and phase encoding gradient L-R, the artifact appeared A-P. The hematomas resolved rapidly, significantly decreasing in size by 1 day (Fig. 2E, F). Mild ipsilateral (or sometimes bilateral) ventricle enlargement was apparent at 2 weeks (Fig. 2G, H). Saline injection was associated with only very small foci of blood accumulation (Fig. 2I). MR images after injection of 50 μL blood into medial striatum of adult mouse brain had a similar appearance to those obtained following acute PVH/IVH in neonates but was associated with less spread into tissue (Fig. 2J). As in newborns, by 1 day the site of blood injection was hardly apparent (not shown).

We quantified and compared the hematoma volume on MRI and histologic sections immediately (15–30 min) and 4 hours following the blood injection into newborn mouse brain (Fig. 3). On MRI there was a significant decrease in size of the hematoma by 4 hours. On histologic examination there was no significant difference in size at the 2 time points. In comparison to MRI, histological preparations showed that blood was in a much more confined region of the periventricular tissue. Although the ventricles were filled with blood, they were only minimally expended. Therefore MRI overestimates the size of the hematoma, but reliably documents the location and allows in vivo documentation of a standard hematoma size. All mice used for quantitative analyses had a similar MR appearance initially.

Histologic Features of PVH/IVH in Neonatal Mice

Examination of the normal mouse brain at 1 to 2 days of age, the time at which blood would be injected, showed that the large elongated cells of the pseudostratified ventricular zone occupied a ~50-μm-thick layer. The smaller, rounder subventricular zone cells over the caudatoputamen (the ganglionic eminence) were packed in a dense layer up to 300-μm thick. Rare mitotic figures could be identified along the ventricle wall and many

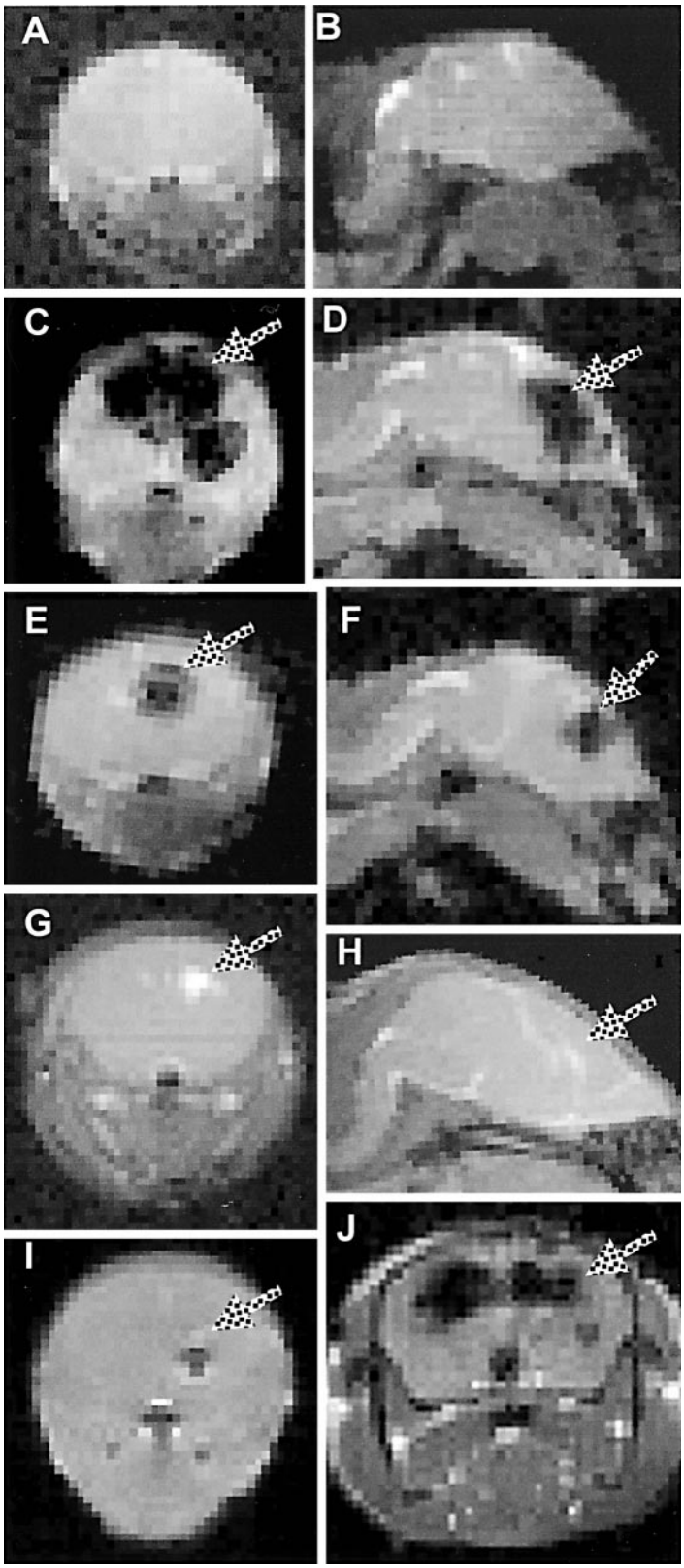

Fig. 2. T2-weighted MR (MT-FLASH) showing coronal (**A, C, E, G, I, J**) and sagittal images (**B, D, F, H**) of mouse brain. Normal 1-day mouse brain is shown in (**A**) and (**B**). One hour following blood injection (15 μL), the hematoma in the striatum (arrow) and ventricles appears dark (**C, D**). A similar but less extensive change is seen in adult mouse brain 1 hour after injection of 50 μL blood (**J**). One hour after saline (15 μL) injection (**I**) into 1-day mouse brain, a small blood collection due to the needle damage is evident (arrow). The injected hematomas resolve rapidly as shown by a significant decrease in size by 1 day (**E, F**) (arrow). By 2 weeks, only a small fluid-filled cavity and/or slightly enlarged ipsilateral ventricle (bright area, arrow) is evident (**G, H**).

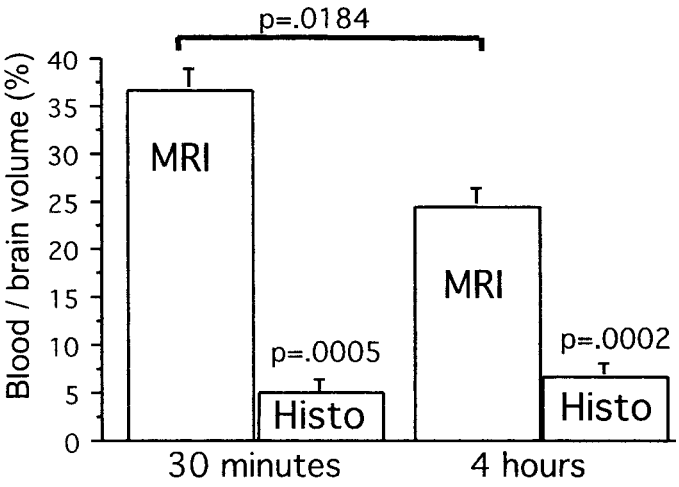

Fig. 3. Proportionate hematoma size on MR images and histological sections 30 min and 4 hours following blood injection into newborn mouse brain. On sequentially imaged mice there was a significant difference in the apparent size of the blood collection between the 2 time points (paired *t*-test, $p < 0.02$). MR images consistently displayed an apparent hematoma size that was significantly larger than the true hematoma size evident on the histologic sections (paired *t*-test, $p < 0.0001$).

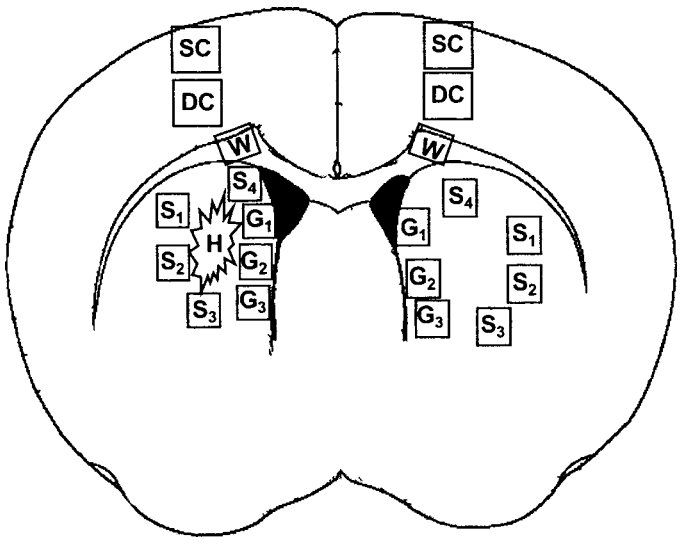

Fig. 4. Schematic diagram of mouse brain showing areas in which cells were counted following blood injection. For quantification of proliferating cells, Ki67-immunolabeled nuclei and bisbenzimide-stained nuclei were counted in the periventricular germinal matrix (G1, G2, and G3), striatum (S1, S2, S3, and S4) adjacent to the hematoma (H), white matter (W), deep cerebral cortex (DC), and superficial cerebral cortex (SC). GFAP immunoreactivity, an indicator of reactive astrogliosis, was assessed semiquantitatively in the same regions. To evaluate cell death and inflammation, TUNEL-positive cells, neutrophils, and RCA-1 labeled microglia were counted in striatum (S1, S2, S3, and S4) adjacent to the hematoma. All assessments were made bilaterally.

more were in the subventricular zone. Scattered apoptotic bodies were present in the subventricular zone. The germinal tissue of the ganglionic eminence was largely gone by 7 days and absent by 28 days, confirming prior observations that the mouse lateral ventricular wall resembles that of adults by 15 days (28). A few ciliated ependymal cells were apparent along the roof of the ventricle by 3 days and many were present along the lateral wall by 7 to 9 days. Their appearance coincided with involution of the ventricular and subventricular zones. Long processes of radial glial cells were apparent on the GFAP-immunostained sections (29) extending into the white matter at the roof of the ventricle and into the caudatoputamen along the wall of the ventricle at 2 days. Far fewer cells with long processes were evident at 7 days. During this involution period many apoptotic bodies were present.

Qualitative and quantitative assessments of brain changes following blood injection were studied in the germinal matrix of the ganglionic eminence, the caudatoputamen, the white matter at the roof of the lateral ventricle, and the dorsal cerebral cortex (Fig. 4). From hours to 2 days after blood injection, damaged brain surrounding the hematoma appeared pale on H&E stain due to edema. The irregular hematoma was located in striatum and GM with extension into the ventricles (Fig. 5A–C). Acutely, hematomas were characterized by single or multiple contiguous collections of blood cells and blood cells mixed with GM cells. These collections were often continuous with intraventricular blood collections because ventricular zone was split. It was difficult to assess ependyma in the blood-filled ventricles. At 1 day, scattered neurons with hypereosinophilic cytoplasm were evident within the damaged striatum. After 1 day, pale-stained degenerating erythrocytes and fragmented nuclear debris were seen. By 7 days, no blood or edema could be identified in the tissue. The hematoma site was difficult to find with the exception of scattered hemosiderin-containing macrophages. The ventricles were slightly enlarged at 28 days.

Cell Proliferation and Cell Death

Counts of proliferating cells were made in several regions of brain adjacent to and distant from the site of the hematoma (Fig. 4). In normal brain, large proportions of cells were Ki67-positive (Fig. 5D–G) in the GM and white matter from 8 hours to 28 days. Fewer proliferating cells were identified in the striatum and cortex. In comparison to intact and saline-injected controls we observed that the proportion of proliferating cells in the GM significantly decreased 8 hours, 2 and 7 days (but not 1 day) after PVH/IVH bilaterally (Fig. 6). In the white matter (corpus callosum and external capsule), decreased cell proliferation was observed bilaterally from 8 hours to 7 days following PVH/IVH. The cerebral cortex showed a

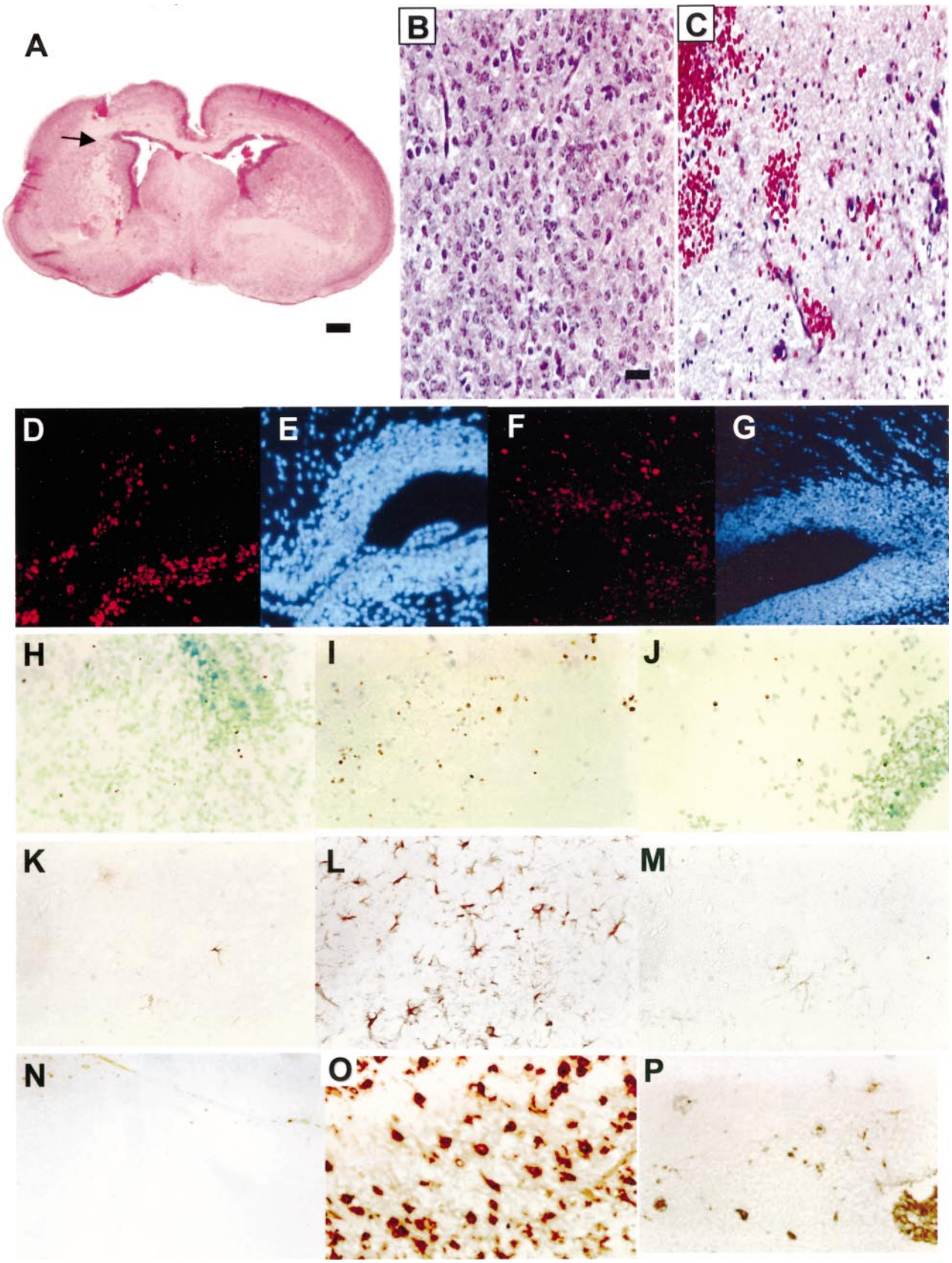

Fig. 5. Photomicrographs of histopathologic features following blood injection into newborn mouse brain. **A:** Low magnification photomicrograph of mouse brain coronal section (H&E stain) at the site of blood injected into the striatum adjacent to the

significant decrease in cell proliferation bilaterally 1 to 2 days after PVH/IVH. The striatum did not show significant change in cell proliferation at any time point.

TUNEL-positive dying cells (Fig. 5H–J) were infrequent in the normal control tissue and contralateral to the hematoma. Ipsilateral to the hematoma more TUNEL-positive dying cells were observed in the striatum and GM 1 and 2 days after PVH/IVH (Fig. 7). Rare, scattered Fluoro-Jade-stained dying neurons, corresponding to hypereosinophilic neurons, were observed in the striatum 1 to 2 days after PVH/IVH and thereafter (data not shown). Cells that stained weakly with Fluoro-Jade were evident in the striatum, cortex of ipsilateral and contralateral hemisphere, and the septum, but these were not obviously dying cells.

In normal brains, astrocytes were immunoreactive for GFAP around blood vessels in the striatum and cerebral cortex and also among axons in the white matter (Fig. 5K–M), beginning at 7 days. Radial glia were immunoreactive for GFAP at 2 to 7 days. Following PVH/IVH, slightly hypertrophic astrocytes were evident at 2 days. Semiquantitative assessment (Fig. 7) showed that the astrocyte reaction was maximal 2 to 7 days after PVH/IVH in the ipsilateral striatum, 2 to 28 days in the ipsilateral white matter, and 7 to 28 days in contralateral white matter. We could not determine specifically whether radial glia cells were disrupted except at the site of the hematoma.

Inflammation

RCA-1 labeling of microglia (Fig. 5N–P) was not evident in normal brain. By 8 hours after PVH/IVH some reactive microglia with narrow cell bodies and branched processes were evident. Their quantity was maximal at 2 to 7 days and had decreased by 28 days (Fig. 7). By 7 days there were round macrophages adjacent to the hematoma. Neutrophils, evident with H&E staining and Gr1 immunostaining, were present in the brain tissue surrounding the hematoma in very small quantities only at 1 to 2 days (1.6 ± 1.5 and 2.4 ± 1.8, respectively, per count region). Immunolabeling with anti-CD3, CD3ε, CD4, and CD8 antibodies showed only very few scattered lymphocytes in the vicinity of the hematoma 2 to 7 days after blood injection (not shown).

DISCUSSION

Animal models are needed to study the pathogenesis of brain damage after PVH/IVH. Intraventricular hemorrhage has been induced using glycerol to create intracranial hypotension in prematurely born rabbits (27 to 30 days gestation) (30). Injection of blood into newborn dog brains has been used to study the effect of acute ventricular distension on the surrounding blood flow patterns (31). Dog models have played an important role in understanding the physiologic factors that predispose to PVH/IVH (2). A mouse model of neonatal hypoxia develops superficial foci of bleeding unlike those seen in humans (32). These studies have been concerned with the physiologic processes and structural features that allow PVH/IVH but not the tissue reactions. In this study, we developed a novel model of PVH/IVH in newborn mouse by injection of autologous whole blood into periventricular tissue including GM and striatum. All mice exhibited extension of the hematoma into the ventricles. Therefore, this model corresponds to grade III/IV PVH/IVH as defined by imaging studies in premature infants (33). This model provides an opportunity to study mechanisms of cellular injury after PVH/IVH.

Histological examination showed that MRI was capable of accurately localizing the hematoma to the periventricular region and the ventricle. MRI allows us to ascertain the size and site of the acute hematoma regardless of the subsequent survival period. There are few studies of human infants with PVH/IVH using MRI. T2-weighted fast spin echo MRI is more sensitive than ultrasound for detecting small sites of hemorrhage (34, 35). The MRI features we observed in mice are similar. However, MRI consistently showed a larger hematoma volume than the histologic preparation. This suggests that hypointensity in the MR image is due to diffusing hemoglobin from lysed cells and/or the large susceptibility effect of paramagnetic hemoglobin. Sequential studies after PVH/IVH

←

periventricular germinal matrix (arrow). The lateral ventricles are enlarged bilaterally and contain a small quantity of blood 4 hours after injection (Bar = 0.5 mm). **B:** Intact newborn medial striatum exhibits tightly packed immature neurons (Bar = 25 μm for panels B–P). **C:** Damaged striatum adjacent to hematoma 2 days after PVH/IVH exhibits fewer neurons, small collections of erythrocytes, and mild pallor due to edema. **D:** Ki67 immunolabeling with Cy3 detection shows abundant proliferating cells (bright red) in the normal germinal matrix at the angle of the lateral ventricle. **F:** Far fewer cells are seen in the age-matched brain, 1 day after blood injection. **E, G:** Bisbenzimide-stained nuclei of same fields respectively. TUNEL showing rare dying cells (brown) in normal newborn striatum (**H**), in striatum adjacent to hematoma (**I**), and in contralateral striatum (**J**) 2 days after PVH/IVH. GFAP immunolabeling shows scattered stellate astrocytes in normal brain (**K**), an increased quantity and size of astrocytes adjacent to the hematoma (**L**) 2 days after blood injection, and few labeled cells in striatum contralateral to the hematoma (**M**). RCA-1 lectin staining shows a negligible number of microglial cells in normal striatum (**N**), an abundance of round macrophages, and plump activated microglia adjacent to the hematoma (**O**) 2 days after blood injection, mild activation of cells in striatum contralateral to the hematoma (P).

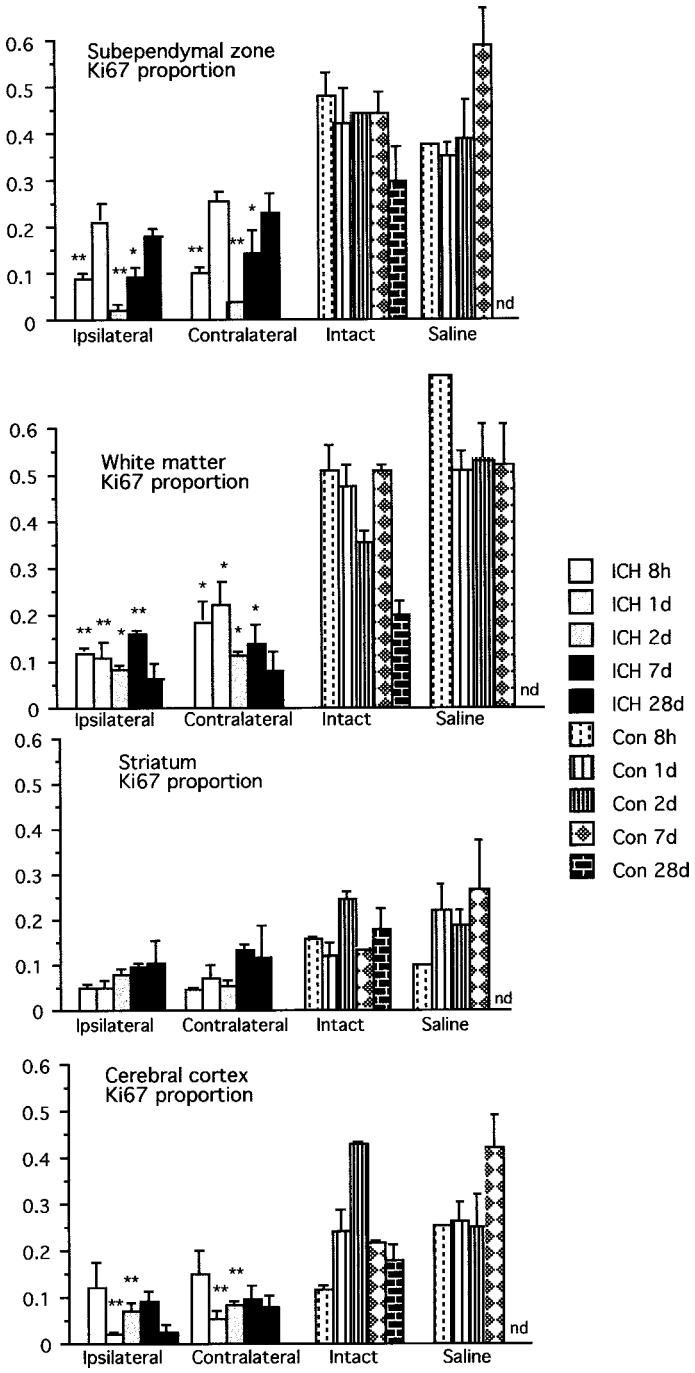

Fig. 6. Bar graphs showing the proportion of proliferating cells (calculated by the number of Ki67-immunoreactive nuclei/total bisbenzimide-stained nuclei) in various regions of mouse brain (see Fig. 4) at sequential times after blood injection. In intact control mice the highest proportions were observed in germinal matrix (subependymal zone). The quantities were negligible by 28 days age, by which time the germinal matrix periventricular white matter had involuted. There was no change following injection of saline. Following injection of blood, the proportion of proliferating cells decreased in the ipsilateral (and to a lesser degree in the contralateral) germinal matrix and white matter from 8 hours to 7 days. There was a moderate decrease in the immature cerebral cortex bilaterally and no change in the striatum. *$p < 0.05$; **$p < 0.01$ ANOVA. Abbreviations: nd = no data; ICH = intracerebral hemorrhage; Con = control.

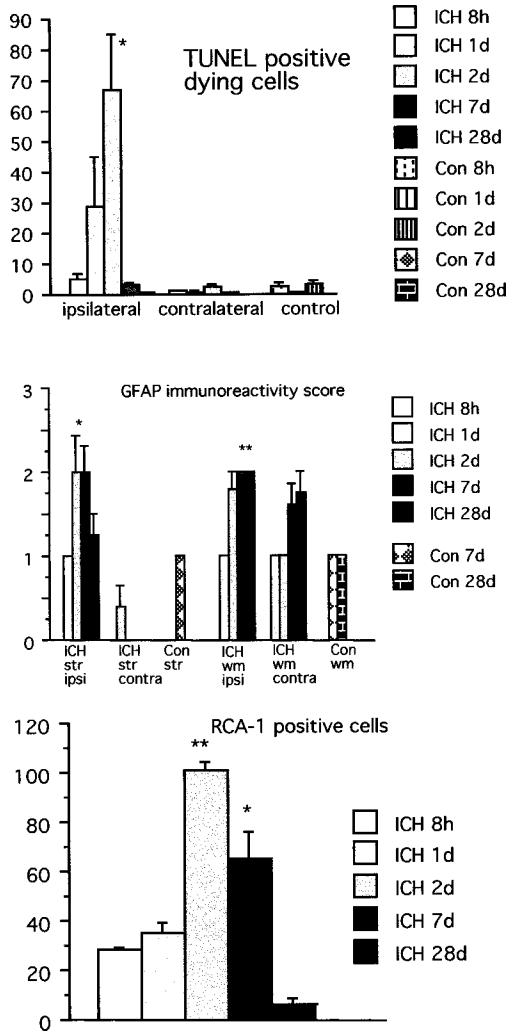

Fig. 7. Bar graphs comparing cell death (upper panel), GFAP immunoreactivity in reactive astrocytes (middle panel), and RCA-1 lectin detection of reactive microglia (lower panel) in control (Con) brains and mouse brains after blood injection (ICH). Rare dying cells were apparent in control brains up to 3 days age (shown as 2 days post-hemorrhage). The number of dying cells was greater adjacent to the hematoma 1 to 2 days after blood injection, but there was no change in the contralateral striatum ($p < 0.05$ ANOVA). GFAP immunoreactivity in astrocytes was negligible in intact control striatum (str) and white matter (wm) prior to 7 days (8 days age). It was increased significantly in the ipsilateral (ipsi) striatum and white matter and slightly in the contralateral (contra) white matter 2 to 7 and 7 to 28 days, respectively, after blood injection (*$p < 0.05$; **$p < 0.01$, Kruskall-Wallis. The quantity of reactive microglia and macrophages binding RCA-1 lectin was negligible in normal brains at all ages (not shown) and was increased 2 to 7 days following the blood injection. *$p < 0.05$; **$p < 0.01$ ANOVA. Abbreviations: ICH = intracerebral hemorrhage, Con = control).

showed rapid dispersion of the blood. Blood in the ventricles is probably washed away by cerebrospinal fluid (CSF). The loosely organized newborn brain might also allow rapid removal of hemoglobin degradation products. MRI showed that the ventricles enlarged slightly weeks after PVH/IVH. This is similar to the hydrocephalus that develops after PVH/IVH in prematurely born infants (36). However, we never observed progression to severe ventricle and head enlargement. When enlargement was unilateral we believe that it is related to mild tissue atrophy.

This study demonstrates that injection of a small quantity of whole blood into the brain of neonatal mice is associated with widespread reduction of cell proliferation, local increase in cell death, diffuse astroglial reaction, and negligible inflammation except for microglial activation. Dying cells, demonstrated by TUNEL and Fluoro-Jade, significantly increased in quantity in the damaged striatum, peaking 2 days following the blood injection. Cell death is expected after brain injury. However, the most impressive finding was that the proportion of proliferating cells decreased ipsilateral and contralateral to the PVH/IVH in the periventricular GM and in white matter. In the newborn rodent, the periventricular germinal region gives rise to glial precursors that migrate into various parts of the ipsilateral cerebral hemisphere (14–16).

Decreased proliferation was observed as early as 8 hours following IVH/PVH. Thus the mechanism of proliferation suppression is likely a direct effect of some mediator from blood or damaged cells and not, for example, through immune cell mediators; the effects of immune activation would probably not be seen until later times after most brain injuries. We expect that the decrease in cell proliferation can be due to one of or a combination of the following mechanisms. The hematoma may cause mechanical destruction, including tearing of cell processes and fragile blood vessels in GM. Cerebral blood flow or venous outflow may be compromised locally (37), in turn leading to ischemic damage (1, 38). Extravasation of blood components, clotting blood, and damaged brain tissue may liberate neurotoxic factors including thrombin, plasminogen, hemoglobin, glutamate, and agents from inflammatory cells (11, 39–43). These agents could spread through ventricular CSF or edematous white matter. High serum concentrations can suppress neuronal proliferation in chick neuroblast cultures (44). Neurotransmitters released in response to injury, such as glutamate and gamma-aminobutyrate (GABA), have also been shown to suppress cell proliferation (45, 46). Together, these mechanical, ischemic, and potentially neurotoxic components constitute a complex insult after PVH/IVH. Because our TUNEL study showed no increase in cell death in the contralateral germinal tissue, it is likely that the factors involved in mediating cell death are different from those that suppress proliferation. Cell proliferation was not significantly decreased at 24 hours. This could be an experimental artifact or there could be a population at cells (e.g. astrocytes or microglia) that begin to proliferate at this time. In the absence of pulse labeling studies with a thymidine analogue, we cannot be certain about this. Longer term suppression could be mediated by other agents produced later e.g. cytokines (47). PVH/IVH can result in enlargement of the lateral ventricles that might compress the adjacent brain tissue causing further damage. This did not seem to be a factor in this experiment.

Our data show that inflammatory cell infiltration has a similar temporal pattern to that in adult rat brain following blood injection (27). However, the number of infiltrating neutrophils and lymphocytes is much lower. Possible reasons are that the chemokines are diluted and washed quickly from the highly hydrated newborn brain (48), that there is an interspecies difference, or that cellular production of chemokines might differ (49). These data suggest that leukocytes probably play a minor role in the brain damage following the PVH/IVH. Microglial reaction, evident beginning at 2 days and persisted up to 28 days was similar to the temporal pattern in adult rats (27).

This study has several potential shortcomings. Newborn mice are very small and they could not be secured in a stereotactic frame. Therefore, the method of freehand blood injection could cause variable brain damage. We used MRI to be sure that blood was indeed injected into the correct location and we only used mice with comparable hematomas. The small size of the brain dictates that diffusible toxic agent(s) have effects in anatomic regions different from those in human brain. For example, a given protein that diffuses 5 mm in both mouse and human brain would produce bilateral effects in mice but only ''focal'' effects in humans. We do not know whether the route of toxic agent spread is through tissue or CSF. The absence of an intact ependymal layer at the age when blood is injected could allow toxic agents to spread directly from CSF into germinal tissue. We did not attempt to determine conclusively whether the suppression of mitotic activity occurs in the ventricular zone or the subventricular zone, although subjectively both would seem to be affected. This is of potential significance because they give rise to different cell types. Nor did we assess whether there was an effect on the differentiation of radial glia, which can act as stem cells as well as migration guides (28). RC2 immunohistochemistry might help address this issue. Finally, cell proliferation was measured indirectly by assessing immunoreactivity for Ki67, which is expressed from late G1 to M phase of the cell cycle and correlates well with thymidine analogue uptake by

proliferating cells (50, 51). The loss of expression does not prove that too few cells were generated because (generally) a surplus of cells is produced. Perhaps the residual proliferative activity was sufficient to produce the necessary cells.

In conclusion, extravasated blood may play an important role in brain damage following PVH/IVH through suppression of cell proliferation in the GM. This is potentially important because MRI studies on humans show that premature birth or periventricular hemorrhage is associated with reduced white matter volume (52). If GM suppression is associated with impaired development of glial precursors it could explain some aspects of the final (sometimes subtle) brain damage following premature birth. The precise molecular and chemical mechanisms remain to be determined but probably are multiple. Complete understanding of the mechanisms of damage associated with PVH/IVH should direct us to new treatment strategies.

ACKNOWLEDGMENTS

This work was supported by grants to Dr. Del Bigio from the Heart and Stroke Foundation of Manitoba, Manitoba Health Research Council, and Children's Hospital Foundation. Dr. Del Bigio holds the MMSF Clinical Research Professorship. Mengzhou Xue and Janani Balasubramaniam have Doctoral Research Awards from CIHR/HSFC. We thank Sharon Allan and Susan Janeczko for technical assistance.

REFERENCES

1. Volpe JJ. Neurology of the newborn. 4th Edition. Philadelphia: W.B. Saunders, 2001
2. Goddard-Finegold J. Experimental models of intraventricular hemorrhage. In: Pape KE, Wigglesworth JS, eds. Perinatal brain lesions. Blackwell Scientific, 1989:115–33
3. Gilles FH, Price RA, Kevy SV, Berenberg W. Fibrinolytic activity in the ganglionic eminence of the premature human brain. Biol Neonate 1971;18:426–32
4. McDonald MM, Johnson ML, Rumack CM, et al. Role of coagulopathy in newborn intracranial hemorrhage. Pediatrics 1984;74: 26–31
5. Van de Bor M, Briet E, Van Bel F, Ruys JH. Hemostasis and periventricular-intraventricular hemorrhage of the newborn. Am J Dis Child 1986;140:1131–34
6. MacDonald BK, Cockerell OC, Sander JW, Shorvon SD. The incidence and lifetime prevalence of neurological disorders in a prospective community-based study in the UK. Brain 2000;123:665–76
7. Rubin RJ, Gold WA, Kelley DK, Sher JP. The cost of disorders of the brain. Washington, DC: National Foundation for Brain Research/Lewin-ICF, 1992
8. Hagberg G, Hagberg B. Antecedents. In: Neville B, Goodman R, eds. Congenital hemiplegia. MacKeith Press, 2000:5–17
9. Towbin A. Mental retardation due to germinal matrix infarction. Science 1969;164:156–61
10. Xue M, Del Bigio MR. Intracortical hemorrhage injury in rats: Relationship between blood fractions and cell death. Stroke 2000; 31:1721–27
11. Xue M, Del Bigio MR. Acute tissue damage after injections of thrombin and plasmin into rat striatum. Stroke 2001;32:2164–69
12. Xi GH, Keep RF, Hoff JT. Erythrocytes and delayed brain edema formation following intracerebral hemorrhage in rats. J Neurosurg 1998;89:991–96
13. Roohey T, Raju TN, Moustogiannis AN. Animal models for the study of perinatal hypoxic-ischemic encephalopathy: A critical analysis. Early Hum Dev 1997;47:115–46
14. Kakita A, Goldman JE. Patterns and dynamics of SVZ cell migration in the postnatal forebrain: Monitoring living progenitors in slice preparations. Neuron 1999;23:461–72
15. Levers TE, Edgar JM, Price DJ. The fates of cells generated at the end of neurogenesis in developing mouse cortex. J Neurobiol 2001; 48:265–77
16. Zhu Y, Li H, Zhou L, Wu JY, Rao Y. Cellular and molecular guidance of GABAergic neuronal migration from an extracortical origin to the neocortex. Neuron 1999;23:473–85
17. Kolb B, Cioe J, Whishaw IQ. Is there an optimal age for recovery from motor cortex lesions? I. Behavioral and anatomical sequelae of bilateral motor cortex lesions in rats on postnatal days 1, 10, and in adulthood. Brain Res 2000;882:62–74
18. Levison SW, Rothstein RP, Romanko MJ, Snyder MJ, Meyers RL, Vannucci SJ. Hypoxia/ischemia depletes the rat perinatal subventricular zone of oligodendrocyte progenitors and neural stem cells. Dev Neurosci 2001;23:234–47
19. Lemire RJ, Loeser JD, Leech RW, Alvord EC. Normal and abnormal development of the human nervous system. Hagerstown, MD: Harper and Row, 1975.
20. Sturrock RR, Smart IH. A morphological study of the mouse subependymal layer from embryonic life to old age. J Anat 1980;130: 391–415
21. Doty FD, Entzminger G, Jr.,Hauck CD, Staab JP. Practical aspects of birdcage coils. J Magn Reson 1999;138:144–54
22. Leo O, Foo M, Sachs DH, Samelson LE, Bluestone JA. Identification of a monoclonal antibody specific for a murine T3 polypeptide. Proc Natl Acad Sci U S A 1987;84:1374–78
23. Mannoji H, Yeger H, Becker LE. A specific histochemical marker (lectin Ricinus communis agglutinin-1) for normal human microglia, and application to routine histopathology. Acta Neuropathol 1986;341–43
24. Brown DC, Gatter KC. Ki67 protein: The immaculate deception? Histopathology 2002;40:2–11
25. Schmued LC, Albertson C, Slikker W, Jr. Fluoro-Jade: A novel fluorochrome for the sensitive and reliable histochemical localization of neuronal degeneration. Brain Res 1997;751:37–46
26. Schmued LC, Hopkins KJ. Fluoro-Jade: Novel fluorochromes for detecting toxicant-induced neuronal degeneration. Toxicol Pathol 2000;28:91–99
27. Xue M, Del Bigio MR. Intracerebral injection of autologous whole blood in rats: Time course of inflammation and cell death. Neurosci Lett 2000;283:230–32
28. Tramontin AD, Garcia-Verdugo JM, Lim DA, Alvarez-Buylla A. Postnatal development of radial glia and the ventricular zone (VZ): A continuum of the neural stem cell compartment. Cereb Cortex 2003;13:580–87
29. Woodhams PL, Basco E, Hajos F, Csillag A, Balazs R. Radial glia in the developing mouse cerebral cortex and hippocampus. Anat Embryol (Berl) 1981;163:331–43
30. Conner ES, Lorenzo AV, Welch K, Dorval B. The role of intracranial hypotension in neonatal intraventricular hemorrhage. J Neurosurg 1983;58:204–9
31. Batton DG, Nardis EE. The effect of intraventricular blood on cerebral blood flow in newborn dogs. Pediatr Res 1987;21:511–15
32. Yoshioka H, Iino S, Sato N, et al. New model of hemorrhagic hypoxic-ischemic encephalopathy in newborn mice. Pediatr Neurol 1989;5:221–25
33. Papile LA, Burstein J, Burstein R, Koffler H. Incidence and evolution of subependymal and intraventricular hemorrhage: A study of infants with birth weights less than 1,500 gm. J Pediatr 1978; 92:529–34

34. Felderhoff-Mueser U, Rutherford MA, Squier WV, et al. Relationship between MR imaging and histopathologic findings of the brain in extremely sick preterm infants. AJNR Am J Neuroradiol 1999; 20:1349–57
35. Maalouf EF, Duggan PJ, Counsell SJ, et al. Comparison of findings on cranial ultrasound and magnetic resonance imaging in preterm infants. Pediatrics 2001;107:719–27
36. Hudgins RJ. Posthemorrhagic hydrocephalus of infancy. Neurosurg Clin N Am 2001;12:743–51
37. Kingman TA, Mendelow AD, Graham DI, Teasdale GM. Experimental intracerebral mass: Time-related effects on local cerebral blood flow. J Neurosurg 1987;67:732–38
38. Volpe JJ. Intraventricular hemorrhage in the premature infant–current concepts. Part 1. Ann Neurol 1989;25:3–11
39. Lee KR, Colon GP, Betz AL, Keep RF, Kim S, Hoff JT. Edema from intracerebral hemorrhage: The role of thrombin. J Neurosurg 1996;84:91–96
40. Mendelow AD. Mechanisms of ischemic brain damage with intracerebral hemorrhage. Stroke 1993;24(Suppl I):I-115–I-117
41. Murphy P. The neutrophil. New York: Plenum Medical Book Co., 1976
42. Wang X, Mori T, Sumii T, Lo EH. Hemoglobin-induced cytotoxicity in rat cerebral cortical neurons: Caspase activation and oxidative stress. Stroke 2002;33:1882–88
43. Xi GH, Wagner KR, Keep RF, et al. Role of blood clot formation on early edema development after experimental intracerebral hemorrhage. Stroke 1998;29:2580–85
44. Barakat I, Labourdette G, Sensenbrenner M. Inhibitory effects of fetal calf serum on proliferation of chick neuroblasts in culture. Dev Neurosci 1983;6:169–83
45. Cameron HA, Hazel TG, McKay RD. Regulation of neurogenesis by growth factors and neurotransmitters. J Neurobiol 1998;36:287–306
46. Luk KC, Sadikot AF. GABA promotes survival but not proliferation of parvalbumin-immunoreactive interneurons in rodent neostriatum: An in vivo study with stereology. Neuroscience 2001;104:93–103
47. Lee SC, Dickson DW, Brosnan CF. Interleukin-1, nitric oxide and reactive astrocytes. Brain Behav Immun 1995;9:345–54
48. Agrawal HC, Davis JM, Himwich WA. Developmental changes in mouse brain: Weight, water content and free amino acids. J Neurochem 1968;15:917–23
49. Anthony D, Dempster R, Fearn S, et al. CXC chemokines generate age-related increases in neutrophil-mediated brain inflammation and blood-brain barrier breakdown. Curr Biol 1998;8:923–26
50. Yu CC, Filipe ML. Update on proliferation-associated antibodies applicable to formalin-fixed paraffin-embedded tissue and their clinical applications. Histochem J 1993;25:843–53
51. Scott RJ, Hall PA, Haldane JS, et al. A comparison of immunohistochemical markers of cell proliferation with experimentally determined growth fraction. J Pathol 1991;165:173–78
52. Nosarti C, Al-Asady MH, Frangou S, Stewart AL, Rifkin L, Murray RM. Adolescents who were born very preterm have decreased brain volumes. Brain 2002;125:1616–23

Received March 24, 2003
Revision received July 29, 2003
Accepted July 31, 2003